Research

Oxidative stress accelerates intestinal tumorigenesis by enhancing 8-oxoguanine-mediated mutagenesis in MUTYH-deficient mice

Mizuki Ohno,[1] Noriko Takano,[1] Kyoko Hidaka,[1,2] Fumiko Sasaki,[1] Kazumi Yamauchi,[1,3] Yasunobu Aoki,[4] Takehiko Nohmi,[5] Yusaku Nakabeppu,[6,7] Yoshimichi Nakastu,[1] and Teruhisa Tsuzuki[1]

[1]*Department of Medical Biophysics and Radiation Biology, Faculty of Medical Sciences, Kyushu University, Fukuoka, Fukuoka 812-8582, Japan;* [2]*Center for Fundamental Education, The University of Kitakyushu, Kitakyushu, Fukuoka 802-8577, Japan;* [3]*Department of Radiobiology, Institute for Environmental Sciences, Kamikita, Aomori 039-3212, Japan;* [4]*Health and Environmental Risk Division, National Institute for Environmental Studies, Tsukuba, Ibaraki 305-8506, Japan;* [5]*Division of Genetics and Mutagenesis, National Institute of Health Sciences, Kawasaki, Kanagawa 210-9501, Japan;* [6]*Division of Neurofunctional Genomics, Department of Immunobiology and Neuroscience, Medical Institute of Bioregulation, Kyushu University, Fukuoka, Fukuoka 812-8582, Japan;* [7]*Japan Society for the Promotion of Science, San Francisco Office, Berkeley, California 94704, USA*

Oxidative stress–induced DNA damage and its repair systems are related to cancer etiology; however, the molecular basis triggering tumorigenesis is not well understood. Here, we aimed to explore the causal relationship between oxidative stress, somatic mutations in pre-tumor-initiated normal tissues, and tumor incidence in the small intestines of MUTYH-proficient and MUTYH-deficient mice. MUTYH is a base excision repair enzyme associated with human colorectal cancer. Mice were administered different concentrations of potassium bromate ($KBrO_3$; an oxidizing agent)–containing water for 4 wk for mutagenesis studies or 16 wk for tumorigenesis studies. All *Mutyh*$^{-/-}$ mice treated with >0.1% $KBrO_3$ developed multiple tumors, and the average tumor number increased dose dependently. Somatic mutation analysis of *Mutyh*$^{-/-}$/*rpsL* transgenic mice revealed that G:C > T:A transversion was the only mutation type correlated positively with $KBrO_3$ dose and tumor incidence. These mutations preferentially occurred at 5′G in GG and GAA sequences in *rpsL*. This characteristic mutation pattern was also observed in the genomic region of *Mutyh*$^{-/-}$ tumors using whole-exome sequencing. It closely corresponded to signature 18 and SBS36, typically caused by 8-oxo-guanine (8-oxoG). 8-oxoG-induced mutations were sequence context dependent, yielding a biased amino acid change leading to missense and stop-gain mutations. These mutations frequently occurred in critical amino acid codons of known cancer drivers, *Apc* or *Ctnnb1*, known for activating Wnt signal pathway. Our results indicate that oxidative stress contributes to increased tumor incidence by elevating the likelihood of gaining driver mutations by increasing 8-oxoG-mediated mutagenesis, particularly under MUTYH-deficient conditions.

[Supplemental material is available for this article.]

Oxidative stress reflects a cellular consequence of an imbalance between reactive oxygen species (ROS) generation and a biological system's ability to detoxify the resulting damage (Sies 2015). It is considered an important etiologic factor in tumor initiation (Ames 1983; Waris and Ahsan 2006). ROS are constantly produced in vivo through normal cellular metabolism; however, their production is further enhanced during infection, inflammation, aging, or exposure to environmental factors, including ionizing radiation or chemicals (Sauer et al. 2001). Various types of oxidatively damaged DNA are produced when ROS attack nucleic acids, resulting in mutations (Maynard et al. 2009). However, molecular mechanisms underlying ROS-triggered tumorigenesis remain unknown.

Of the four DNA nucleobases, guanine is most susceptible to oxidation, and 8-oxo-7,8-dihydroguanine (8-oxoguanine [8-oxoG]) is its major oxidized form (Kasai and Nishimura 1984). 8-oxoG is a potent premutagenic lesion because it can form a stable base pair with adenine and cytosine, resulting in the G:C > T:A transversion mutation (Shibutani et al. 1991). The nuclear DNA of human and mouse normal somatic cells have more than 10,000 8-oxoG residues (Ohno et al. 2006). The amount of 8-oxoG in the DNA of steady-state living cells is determined based on a dynamic equilibrium between its generation through oxidation and removal by the DNA repair system. Therefore, exposure of cells to excess oxidative stress or dysregulations in the repair system results in biological consequences of 8-oxoG, including an increase in mutation frequency (MF) in both somatic and germline cells (Ohno et al. 2014; Ohno 2019).

Common molecular mechanisms for preventing 8-oxoG-mediated mutagenesis have been reported across a range of organisms, from bacteria to mammals (Tsuzuki et al. 2007; Boiteux et al. 2017; Nohmi 2018). In mice and humans, three enzymes, namely, NUDT1 (also known as MTH1), OGG1, and MUTYH, act in coordination to reduce mutations. NUDT1 hydrolyzes 8-oxo-dGTP to

Corresponding author: mizuki.ohno.700@m.kyushu-u.ac.jp
Article published online before print. Article, supplemental material, and publication date are at https://www.genome.org/cgi/doi/10.1101/gr.278326.123.

8-oxo-dGMP to prevent the incorporation of oxidized nucleotides into DNA during replication. OGG1 is a DNA glycosylase that recognizes the 8-oxoG:C pair in double-stranded DNA and initiates base excision repair by excising the 8-oxoG base (Radicella et al. 1997; Rosenquist et al. 1997). MUTYH is an adenine DNA glycosylase, which excises misincorporated adenine opposite of 8-oxoG in the template strand during DNA replication as the first step of base excision repair (McGoldrick et al. 1995). The deficiency in the enzymatic activities of NUDT1 or/and OGG1 increases 8-oxoG levels in the DNA, resulting in MUTYH repair target 8-oxoG:A mispairs. Mice lacking one of these enzymes are cancer-prone later in age (Sakumi et al. 2003; Xie et al. 2004; Sakamoto et al. 2007), whereas TOY mice, which lack all three of the genes *Nudt1*, *Ogg1*, and *Mutyh*, develop spontaneous tumors at a younger age and have a short lifespan (Ohno et al. 2014). TOY mice show a high spontaneous germline mutation rate, showing significantly increased G:C > T:A mutations. The administration of potassium bromate ($KBrO_3$), an oxidizing reagent, increases tumor frequency in the small intestines of *Mutyh*-deficient mice (Sakamoto et al. 2007). MUTYH-associated polyposis (MAP) is a human colorectal cancer predisposition syndrome caused by biallelic germline mutations in *MUTYH* (Al-Tassan et al. 2002; Poulsen and Bisgaard 2008). MAP tumors show distinct molecular features, including frequent G:C > T:A mutations in cancer-related genes or genomic regions (Al-Tassan et al. 2002; Poulsen and Bisgaard 2008; Rashid et al. 2016; Pilati et al. 2017; Viel et al. 2017). MUTYH may play an important role in the prevention of oxidative stress–induced tumors in humans.

Human somatic cells acquire many mutations during development and aging. Recent studies have reported the prevalence of cancer-associated mutations in normal tissues, which accumulate with aging (Risques and Kennedy 2018; Evans and Degregori 2021). Somatic MF in normal tissues is influenced by internal or external mutagens from a young age and can be an important predictor of subsequent tumor incidence in the same organ. Therefore, we aimed to examine whether the increase in somatic MF in normal tissues of oxidatively stressed mice preceded tumor development and whether it was correlated to tumor incidence at a later age in a mouse model of an intestinal tumor. However, quantitative and qualitative analyses of somatic mutations in nontumor normal tissues are challenging because spontaneous MF is extremely low for detection using simple massively parallel sequencing. Therefore, herein, we used *rpsL* transgenic (Tg) mice, which harbor multiple copies of reporter genes, for an in vivo mutagenesis assay (Gondo et al. 1996; Egashira et al. 2002).

Here, we examined correlations among oxidative stress level, somatic MF, and spectra in pre-tumor-initiated normal tissues and tumor frequency at the later stage. First, we analyzed effects of oxidative stress levels on tumor incidence in $Mutyh^{+/+}$, $Mutyh^{+/-}$, and $Mutyh^{-/-}$ mice. Next, we analyzed the somatic MF and spectra in normal precancerous tissues using $Mutyh^{+/+}$/*rpsL*-Tg and $Mutyh^{-/-}$/*rpsL*-Tg mice. Finally, we conducted whole-exome sequencing (WES) analysis to identify unique somatic mutations acquired during tumor development and explored mutation patterns and driver mutations in $Mutyh^{-/-}$ tumors.

Results

Analysis of oxidative stress–induced tumors

To assess the causal effect of oxidative stress on tumorigenesis, we analyzed tumor frequency in small intestines of $Mutyh^{+/+}$, $Mutyh^{+/-}$, and $Mutyh^{-/-}$ mice after chronic administration of $KBrO_3$. Mice were administered 0.5%, 0.1%, 0.15%, or 0.2% $KBrO_3$-containing water or regular water for the nontreated control for 16 wk from 4 wk of age (Fig. 1A). No tumors were observed in nontreated control groups and 0.5% $KBrO_3$-treated groups regardless of the *Mutyh* genotype. Notably, $Mutyh^{-/-}$ mice showed a remarkable elevation in tumor number with an increase in $KBrO_3$ dose (Fig. 2A; Table 1). For instance, the average tumor number per mouse was 8.8, 41.6, and 61.9 in the 0.1%, 0.15%, and 0.2% $KBrO_3$-treated groups, respectively, whereas those in $Mutyh^{+/+}$ and $Mutyh^{+/-}$ mice were 0.9 ± 0.6 and 3.2 ± 1.3, respectively, even with treatment with the highest $KBrO_3$ dose. Although $Mutyh^{+/+}$ and $Mutyh^{+/-}$ mice showed substantially lower tumor numbers than $Mutyh^{-/-}$ mice, a significant positive correlation between tumor number and $KBrO_3$ dose was observed in all genotypes ($P < 0.0001$, $\rho = 0.9028$, 0.5865, and 0.5815 in $Mutyh^{-/-}$, $Mutyh^{+/-}$, and $Mutyh^{+/+}$, respectively) (Supplemental Table S1). Most tumors were detected predominantly in regions corresponding to the duodenum and jejunum, showing nonpolypoid growth with almost the same height as around normal villi (Fig. 1B–F; Supplemental Fig. S1), consistent with the findings of our previous studies (Sakamoto et al. 2007; Isoda et al. 2014).

When focusing on the tumor prevalence, namely, percentage of mice having at least one tumor, we observed the obvious $KBrO_3$ dose effect in all genotypes (Table 1; Fig. 2B); 100% of $Mutyh^{-/-}$ mice developed tumors at doses of ≥0.1%. In $Mutyh^{+/+}$ mice, it gradually increased with $KBrO_3$ dose; however, ∼20% of mice treated with the highest dose did not develop tumors during the experimental period. In $Mutyh^{+/-}$ mice, although the average tumor number was small, the plot pattern of tumor prevalence by KBrO3 dose was close to that of $Mutyh^{-/-}$ mice.

To evaluate effects of longer exposure to oxidative stress on tumorigenesis in wild-type mice, $Mutyh^{+/+}$ mice were administered 0.15% $KBrO_3$ for 40 wk. Eleven out of 12 mice (92%) developed one to four tumors (2.42 ± 1.38); the mean tumor number per mouse was 2.69 times higher than that of the 16-wk treated group (Wilcoxon test, $P = 0.003$) (Supplemental Fig. S2). Thus, the dose and administration period of oxidative stress may affect tumor incidence even under the MUTYH-proficient condition.

Analysis of somatic mutations in the normal precancer tissues by reporter gene assay

To evaluate the MF during the pre-tumor-initiation phase, we conducted a *rpsL* reporter gene assay using normal small intestinal tissues obtained from mice treated with $KBrO_3$ for 4 wk. Here, MF was defined as the fraction of mutated *rpsL* gene among the total *rpsL* gene loci analyzed, namely, per locus MF.

Total MF in $Mutyh^{+/+}$ and $Mutyh^{-/-}$ mice in the control groups was $1.41 \times 10^{-5} \pm 0.71$ and $2.07 \times 10^{-5} \pm 0.47$, respectively (Table 2; Fig. 3A; Supplemental Table S2). The basal level MF in $Mutyh^{-/-}$ mice was approximately 1.5 times higher than that in $Mutyh^{+/+}$ mice; however, there was no statistically significant difference. All the $KBrO_3$-treated groups showed relatively higher MF compared with those in the matched control group in both genotypes. The mean total MF in $Mutyh^{+/+}$ and $Mutyh^{-/-}$ mice in the 0.2% $KBrO_3$-treated groups was $2.34 \times 10^{-5} \pm 1.61$ and $4.67 \times 10^{-5} \pm 0.34$, respectively. However, using Steel's test, no statistically significant difference was detected in any pairs compared with the matched control.

To determine the site and spectra for each mutation, *rpsL* coding regions from all mutant colonies were sequenced (Table 2). In $Mutyh^{+/+}$ mice, insertion/deletion (indel) mutations were more frequently observed than base substitutions, accounting for ∼70% of

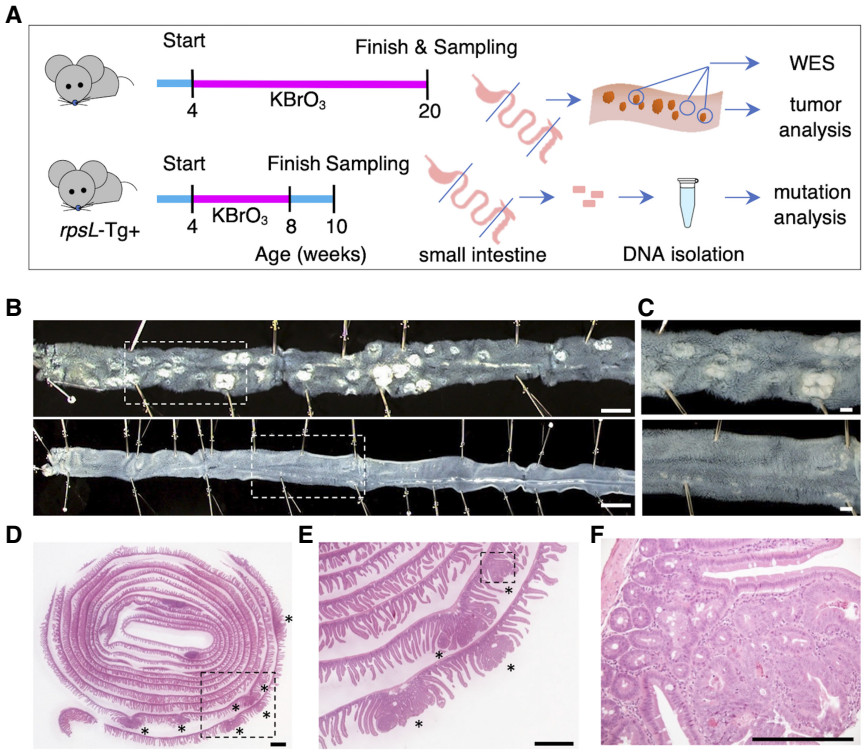

Figure 1. Experimental design and tumor analysis. (*A*) Experimental design of $KBrO_3$ administration. Schedule for tumor analysis (*upper*) for *rpsL* mutation analysis (*lower*). Blue and magenta lines indicate the administration period of regular water or $KBrO_3$-containing water, respectively. (*B*) Formalin-fixed small intestines (duodenum to ileum, *right* to *left*) collected from 0.15% $KBrO_3$-treated mice. *Upper* panel: specimens from *Mutyh*$^{-/-}$ mouse. Multiple tumors (white spot-like parts) are observed. *Lower* panel: specimens from *Mutyh*$^{+/+}$ mouse. No visible tumor was observed. Scale bars indicate 1 cm. (*C*) Magnified images of *B*. The scale bar indicates 1 mm. (*D*–*F*) HE-stained section of StR of the small intestine (Supplemental Methods) of 0.15% $KBrO_3$-treated *Mutyh*$^{-/-}$ mice. The scale bar indicates 1 mm. (*D*) Multiple tumors (asterisks) at the outer side correspond to the region of the duodenum and jejunum. (*E*) Magnified view of the marked area in *D*, with >1-mm sized tumors (polyp-like form) among normal villi. (*F*) Magnified view of the marked area in *E*.

all mutations (Table 2; Fig. 3B). In *Mutyh*$^{-/-}$ mice, the relative ratio of transversion mutations gradually increased with $KBrO_3$ dose, which accounted for >50% of the total mutations in the 0.1%, 0.15%, and 0.2% $KBrO_3$-treated groups (Fig. 3C). This was largely attributed to the increase in G:C>T:A substitutions. Only G:C>T:A substitutions increased with $KBrO_3$ dose in *Mutyh*$^{-/-}$ mice (Table 2; Fig. 3D; Supplemental Fig. S3). The MF of G:C>T:A in 0.2% $KBrO_3$-treated *Mutyh*$^{-/-}$ mice was 2.73×10^{-5}, which was approximately 17 times higher than that of the nontreated control group. A significant positive correlation was detected between the $KBrO_3$ dose and MF of G:C>T:A in *Mutyh*$^{-/-}$ mice (Spearman's rank correlation coefficient, $\rho = 0.765$, $P < 0.0001$) (Supplemental Table S1). Furthermore, an elevation in MF of G:C>T:A was observed in $KBrO_3$-treated *Mutyh*$^{+/+}$ mice. However, it was not statistically significant. No other mutation types showed a positive correlation with $KBrO_3$ dose in *Mutyh*$^{+/+}$ or *Mutyh*$^{-/-}$ mice, except for the total MF in *Mutyh*$^{-/-}$ mice (Fig. 3E–G; Supplemental Table S1). We next ascertained the correlations between each mutation type and tumor frequency. Notably, only the MF of G:C>T:A showed a positive correlation with tumor frequency in *Mutyh*$^{-/-}$ mice (Supplemental Table S1).

To analyze the site distribution and sequence context around mutated sites, base substitution mutations were mapped onto the *rpsL* gene sequence (Supplemental Fig. S4A–D). G:C>T:A mutations detected in $KBrO_3$-treated *Mutyh*$^{-/-}$ mice tended to occur at 5′ guanine in GAA/TTC or GG/CC sites (Supplemental Fig. S4B). In this experiment, G:C>T:A mutations were found at 19 sites, of which six were regarded as hot spots because G:C>T:A mutations were identified multiple times in different mice. All six hot spots contained GAA/TTC or GG/CC sequences. Mutations identified in those sites constituted >70% of all G:C>T:A mutations detected in *Mutyh*$^{-/-}$ mice (Supplemental Fig. S4B). In *Mutyh*$^{+/+}$ mice, G:C>T:A mutations also tended to occur at the same six hot spots (Supplemental Fig. S4D). In contrast, G:C>A:T mutations were predominantly detected at two other hot spots, containing CG/GC and CC/GG sites, regardless of genotype or $KBrO_3$ treatment (Supplemental Fig. S4D).

Analysis of somatic mutations in $KBrO_3$-induced *Mutyh*$^{-/-}$ tumors by WES

To explore whether the characteristic mutation pattern seen in the *rpsL* reporter genes was also observed in the genomic region of *Mutyh*$^{-/-}$ mice, we performed WES analysis. Four tumor samples and two matched normal samples derived from two $KBrO_3$-treated *Mutyh*$^{-/-}$ mice were used. In total, 1073 single-nucleotide

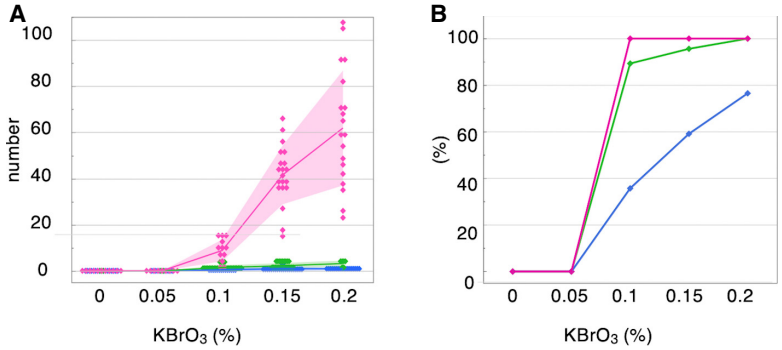

Figure 2. Dose-dependent increase in intestinal tumors in $KBrO_3$-treated mice. Magenta, green, and blue dots and lines indicate the data of *Mutyh*$^{-/-}$, *Mutyh*$^{+/-}$, and *Mutyh*$^{+/+}$, respectively. (*A*) The number of tumors per mouse is plotted based on genotype and $KBrO_3$ dose. The line is drawn through the mean values. The pale-colored bands represent ± SD. (*B*) Tumor prevalence. The percentage of mice with tumor (s) in each study group is plotted against $KBrO_3$ dose.

Table 1. Results of tumor analysis

		$KBrO_3$ concentrations				
Mutyh		0%	0.05%	0.10%	0.15%	0.20%
+/+	Mean tumor number ± SD	0	0	0.4 ± 0.6	0.9 ± 1.0	0.9 ± 0.6
	Tumor prevalence (%)	0	0	35.7	59.1	76.5
	Number of mice analyzed	17	11	14	22	17
+/−	Mean tumor number ± SD	0	0	1.4 ± 0.9	2.2 ± 1.2	3.2 ± 1.3
	Tumor prevalence (%)	0	0	89.3	95.6	100
	Number of mice analyzed	3	3	29	23	6
−/−	Mean tumor number ± SD	0	0	8.8 ± 4.7	41.6 ± 12.7	61.9 ± 24.9
	Tumor prevalence (%)	0	0	100	100	100
	Number of mice analyzed	11	9	12	20	19

variants (SNVs), an average of 268 per tumor, 17 indels, and six multinucleotide substitutions were identified from four tumors (Table 3; Supplemental Table S3). Consistent with the *rpsL* assay, the most frequently observed mutation type was GC > T:A, accounting for 80.5% of total SNVs, followed by G:C > A:T (9.4%), and A:T > G:C (5.7%) (Table 3). The transition/transversion ratio was 0.2.

To analyze the sequence context of the mutated sites, six types of base substitutions were broken down into 96 subtypes, which were all conservable trinucleotide sequences, including 5′ and 3′ flanking bases at mutated sites (Alexandrov et al. 2013). Note that bases of mutated sites were denoted by the pyrimidine bases of the Watson–Crick base pair in accordance with the convention of mutational signature analysis. C > A mutations were preferentially located at the center of trinucleotides of TCT, CCT, CCA, and ACA, followed by TCA, TCC, GCT, GCA, and CCC (Fig. 4A; Supplemental Fig. S5). SNVs were almost equally distributed on both transcribed and nontranscribed strands (Supplemental Fig. S6A,B). Indels and multinucleotide substitutions were less frequently detected than SNVs, with no evidence of instability at short tandem repeats (Supplemental Fig. S6C). In the 1536 pentanucleotide pattern, thymine was frequently located at 5′ and 3′ ends of trinucleotides such as TTCTT or TCCTT (Supplemental Fig. S7).

The mutation pattern of the *Mutyh*$^{-/-}$ tumor detected using WES was consistent with results of the *rpsL* reporter gene assay and the TOY germline mutation pattern (Fig. 4A–C; Supplemental Tables S4, S5). Among the known COSMIC signatures, SBS36, SBS18, and signature 18 (Fig. 4E–G) showed higher values of cosine similarity against the mutation pattern of

Table 2. Mutation frequency based on spectra

Mutyh genotype	+/+					−/−				
								MF ($\times 10^{-5}$)		
$KBrO_3$ (%)	0	0.05	0.1	0.15	0.2	0	0.05	0.1	0.15	0.2
Transition										
G:C > A:T	0.16	0.12	0.92	0.63	–	0.19	0.58	0.74	0.18	–
A:T > G:C	–	0.06	0.04	0.11	0.11	0.13	–	0.16	0.05	–
Transversion										
G:C > T:A	0.08	0.31	0.34	0.28	0.47	0.16	1.02	2.25	2.54	2.73
G:C > C:G	–	–	0.06	–	–	0.04	–	0.03	–	–
A:T > T:A	0.05	–	–	–	–	0.1	–	–	–	–
A:T > C:G	–	–	0.03	–	–	–	–	–	–	–
Indel										
1-bp del (poly(A))	0.49 (0.20)	0.39	0.31 (0.06)	0.7 (0.06)	0.43 (0.14)	0.57 (0.19)	1.33 (0.06)	0.48 (0.05)	0.78 (0.06)	0.49
1 bp ins (poly(A))	–	–	0.02 (0.02)	0.13	–	–	–	0.1 (0.1)	0.1 (0.1)	– –
>2-bp indel	0.64	1.04	0.63	0.83	1.33	0.93	0.87	0.94	1.04	1.46
Others	–	–	–	0.1	–	0.05	–	–	0.07	–
Total	1.41	1.92	2.36[a]	2.78[a]	2.34	2.17[a]	3.79	4.69[a]	4.75[a]	4.67

[a]Total MF including more than two mutations detected in a single Km/Sm-resistant colonies. (–) Not detected.

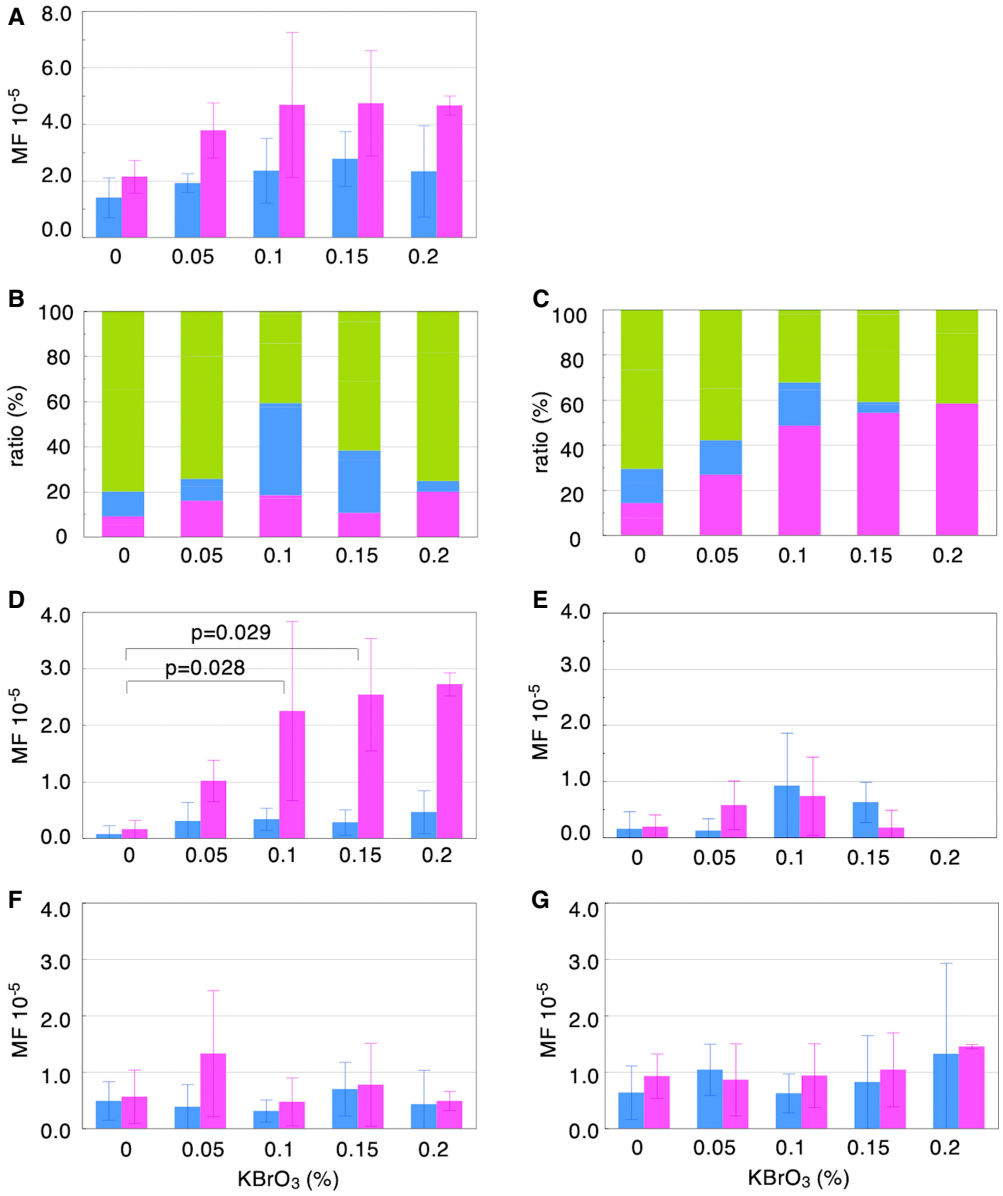

Figure 3. Somatic mutations in the normal intestinal tissues detected using the *rpsL* assay. (*A*) Mutation frequency (MF) in *Mutyh*$^{-/-}$ mice (magenta) and *Mutyh*$^{+/+}$ mice (blue) based on the $KBrO_3$ dose. Mean ± SD. (*B*) The relative ratio of mutation type is shown in the stacked bar chart. Mutations in the *Mutyh*$^{+/+}$ mice. Green, magenta, and blue indicate indels, transversions, and transitions, respectively. (C) Same chart as *B* for *Mutyh*$^{-/-}$ mice. (*D*–*G*) MF is plotted based on the mutation type. Mean ± SD. *Mutyh*$^{-/-}$ mice (magenta) and *Mutyh*$^{+/+}$ mice (blue). Steel's test (vs. $KBrO_3$ 0%; control) was performed, and *P*-values are described in the plot if significant. (*D*) G:C > T:A transversion. (*E*) G:C > A:T transition. (*F*) One-base-pair deletion. (*G*) More than 2-bp indel.

Mutyh$^{-/-}$ mice tumor (0.858, 0.851, and 0.835, respectively) (Supplemental Table S4). These signatures are often found in human cancers with defective MUTYH. Indeed, the mutation pattern of *Mutyh*$^{-/-}$ tumor showed a significant positive correlation with that of human MAP tumors (r = 0.828, $P < 0.0001$) (Fig. 4D; Supplemental Table S5), suggesting a functional commonality of MUTYH in mice and humans.

Functional analysis of the detected mutations revealed that the ratio of nonsynonymous/synonymous was 2.5. In the nonsynonymous mutations, 82% were missense and 12% were stop-gain mutations. This bias toward nonsynonymous mutations could be attributed to the preferred sequence contexts of 8-oxoG. To examine whether the characteristic mutation pattern owing to unrepaired 8-oxoG:A yields any biases in amino acid change, we analyzed the codon and amino acid changes that occurred in the tumors of *Mutyh*$^{-/-}$ mice. The occurrence of base substitutions in each codon sequence largely differed among 64 trinucleotide types, which resulted in a distinct pattern of amino acid change (Supplemental Figs. S8, S9). E > stop (glutamic acid to stop codon) was the most frequently detected type of amino acid change. This was attributed to frequent G > T mutations at the first G in GAA and GAG sequences, both of which code glutamic acid. Following this, K > N, L > I, and D > Y were positioned at the top of the list.

Next, we searched for driver mutations in each tumor. We found G:C > T:A mutations within TCT/AGA sequences in exon

Table 3. Number of variants detected in *Mutyh*$^{-/-}$ tumors using WES

	Tumor ID				
	RY1114 T6	RY1114 T7	RY1115 T2	RY1115 T6	Total
Transition					
G:C>A:T	34	29	26	12	101
A:T>G:C	21	23	12	5	61
Transversion					
G:C>T:A	272	172	297	123	864
G:C>C:G	3	4	3	4	14
A:T>T:A	6	9	2	3	20
A:T>C:G	3	5	2	3	13
SNV total	339	242	342	150	1073
Indel, MNS	5	9	2	8	23
Total	344	251	344	157	1096

(MNS) Multinucleotide substitution.

3 of *Ctnnb1* in three out of four tumors (Supplemental Fig. S10; Supplemental Table S3). These mutations led to S>Y change at the 33rd and 37th amino acids. S>Y was attributed to TCC>TAC and TCT>TAT mutations; this amino acid change was frequently detected here (Supplemental Figs. S8, S9). In one tumor (RY1115-T2), with no *Ctnnb1* mutation, an E>stop mutation in *Hydin*, a candidate cancer driver (Viel et al. 2017), was found at 15% allelic frequency. No other pathogenic mutations were observed in known driver genes frequently mutated in human MAP tumors, such as *Apc*, *Amer1*, *Fat1*, *Fat4*, *Kdm6a*, *Kras*, *Pik3ca*, *Trp53*, *Smad2*, *Smad4*, and *Braf* (Viel et al. 2017).

Finally, we re-evaluated the somatic mutations from the tumor WES using the newly released mouse reference genome mm39 (Supplemental Table S3). The number and pattern of these mutations were nearly identical to those obtained using the mm10 reference genome (Supplemental Fig. S11).

Discussion

Here, we provided compelling evidence that chronic exposure to oxidative stress accelerates tumorigenesis by evoking excessive somatic mutations, particularly under MUTYH-deficient conditions (Tables 1–3; Figs. 1, 2). When treated with 0.2% $KBrO_3$, *Mutyh*$^{-/-}$ mice developed approximately 69 times more tumors than *Mutyh*$^{+/+}$ mice (Table 1). We observed positive correlations between the $KBrO_3$ dose and MF of G:C>T:A, MF of G:C>T:A and tumor incidence, and $KBrO_3$ dose and tumor incidence in *Mutyh*$^{-/-}$ mice. A strong tumor-suppressive role of MUTYH was attributed to preventing oxidative stress–induced mutagenesis, particularly in avoiding 8-oxoG-mediated G:C>T:A transversion (Fig. 3). Thus, we concluded that 8-oxoG:A is the key molecular initiating event triggering intestinal tumorigenesis in *Mutyh*$^{-/-}$ mice. Moreover, sequence context–dependent G:C>T:A mutagenesis yielded biased amino acid change to missense and stop-gain mutations (Supplemental Fig. S9). Our results and human MAP studies (Al-Tassan et al. 2002; Viel et al. 2017) suggest the importance of MUTYH repair function in the prevention of oxidative stress–induced tumorigenesis in both mice and humans.

We previously showed that *Mutyh*$^{-/-}$ mice did not show a remarkable phenotype at a younger age (i.e., before 12 mo) but showed increased spontaneous tumor susceptibility after aging (i.e., after 18 mo) (Sakamoto et al. 2007). For example, eight of 121 mice developed one or two tumors in the small intestines at 18 mo of age. However, no intestinal tumors were observed in 109 age-matched wild-type control mice. In the present study, 100% of *Mutyh*$^{-/-}$ mice treated with >0.1% $KBrO_3$ for 16 wk developed multiple tumors at 5 mo of age; the tumor number per mouse increased with an increase in $KBrO_3$ concentration. This finding suggests that when *Mutyh*$^{-/-}$ mice experience oxidative stress from a younger age, they show a moderate-to-high mutator phenotype and high tumor susceptibility (Tables 2, 3). Furthermore, additional disruption of *Ogg1* in *Mutyh*$^{-/-}$ background increased spontaneous tumor incidence in multiple organs and shortened lifespan compared with *Mutyh* single-knockout mice (Russo et al. 2009; Ohno et al. 2014). Defective OGG1 repair activity leads to the accumulation of 8-oxoG in the genomic DNA (Ohno et al. 2014), subsequently increasing 8-oxo-G:A mismatches during DNA replication. This is a possible reason for the severe phenotype of double-knockout mice. These observations indicate that adverse health effects caused by MUTYH deficiency appear when 8-oxo-G:A mismatch, the repair target of MUTYH, is generated beyond a certain critical level. The risk of colon cancer in patients with MAP increases with age, rapidly elevating after age 50 (Lubbe et al. 2009). An age-dependent increase in oxidative stress could be the cause of this. Indeed, MUTYH-deficient human cells showed high MF when exposed to $KBrO_3$ (Ruggieri et al. 2013; Grasso et al. 2014). Additionally, MFs in the normal intestinal tissues of patients with MAP are higher compared with those in healthy controls (Robinson et al. 2022). Minimizing oxidative stress from a younger age may help in reducing the induction of 8-oxoG and the subsequent formation of 8-oxo-G:A-induced somatic mutations, thereby potentially lowering the risk of tumorigenesis in MAP.

Currently, genotoxic carcinogens are regulated assuming no threshold for their action (Nohmi 2018). We attempted to determine whether this is the case for $KBrO_3$-induced oxidative stress. Our results suggest that a practical threshold for mutagenicity and tumorigenicity existed at doses of 0.05%–0.1% $KBrO_3$ regardless of mice genotype. This is consistent with a previous report showing a practical threshold of mutagenicity in *gpt* delta mice of 0.02%–0.06% (Aoki et al. 2020). Although MUTYH plays a

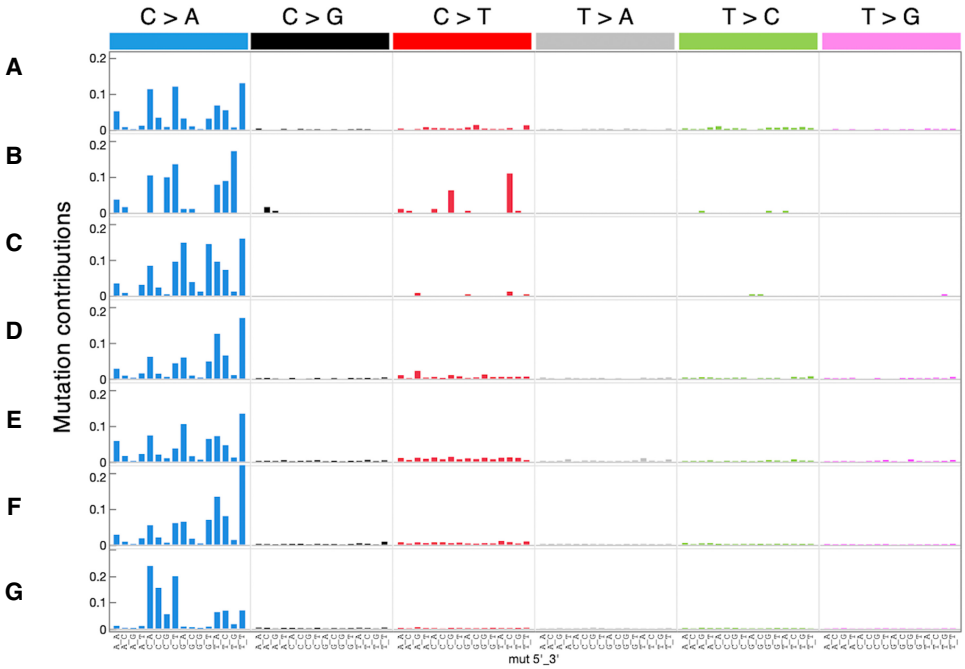

Figure 4. Mutation pattern of $KBrO_3$-induced tumor in *Mutyh*$^{-/-}$ mice. The mutation pattern is displayed based on the 96-base substitution classification defined by the substitution class and sequence context immediately 3′ and 5′ to the mutated base. The *y*-axis indicates the contribution of each mutation to the total mutation number. The *x*-axis indicates 96 trinucleotide types. (*A*) Somatic mutations in the tumor samples of $KBrO_3$-treated *Mutyh*$^{-/-}$ mice detected using WES. (*B*) Somatic mutations were detected in the normal intestinal tissues (pre-tumor-initiation stage) of $KBrO_3$-treated *Mutyh*$^{-/-}$ mice using the *rpsL* assay. (*C*) Mutation pattern of de novo germline mutations detected in TOY mice (Ohno et al. 2014). (*D*) Mutation pattern of tumor samples from human patients with MAP (see Methods). (*E*) Signature 18 in COSMIC mouse ver.2. (*F*) SBS 36 in COSMIC mouse ver.3. (*G*) SBS 45 in COSMIC mouse ver.3.

significant role in the molecular mechanisms underlying the threshold for $KBrO_3$-induced mutagenesis and tumorigenesis in wild-type mice, although it not the only factor involved.

G:C > T:A frequency was affected by the surrounding sequence context. The mutation pattern from *rpsL* and WES indicated that the 5′ G at GG and GAA was frequently mutated. Similar sequence contexts were also preferred in G:C > T:A mutations in the *mutY*$^{-}$ *Escherichia coli* mutator strain (Tajiri et al. 1995; Foster et al. 2015) or wild-type *E. coli* strain harboring *supF* plasmid (Watanabe et al. 2001). Molecular mechanisms underlying the sequence context tendency of G:C > T:A mutation are common among bacteria, mice, and humans. G:C > T:A mutations tended to occur at the same hot spots as in *rpsL* even in $KBrO_3$-treated wild-type mice; therefore, these mutations may not be because of a MUTYH defect. OGG1 repair activity of 8-oxoG in DNA is affected by the surrounding sequence or presence of DNA lesions (Sassa et al. 2012); however, the same mutation pattern was observed in mice lacking both OGG1 and MUTYH (Ohno et al. 2014), possibly because of a physicochemical feature of 8-oxoG in DNA, at least in part. At the 5′ guanine of GG, GA showed lower ionization potential (Sugiyama and Saito 1996), thereby forming preferential oxidation sites in the genome (Fleming and Burrows 2021).

We observed striking similarities between mutation patterns of *Mutyh*$^{-/-}$ tumors and germline mutation detected in TOY mice that lack *Nudt1*, *Ogg1*, and *Mutyh* (Ohno et al. 2014); COSMIC signature 18 and SBS36; and human MAP tumors (Pilati et al. 2017; Viel et al. 2017). Our results provided direct experimental evidence for these signatures being caused by 8-oxoG-induced mutation and for a commonality of MUTYH repair function in mice and humans. SBS45 and SBS4 showed a higher cosine similarity ($r > 0.8$) (Supplemental Table S4) against the mutation pattern of *Mutyh*$^{-/-}$ mice tumor but not of TOY mice. Thus, SBS45 and SBS4 might be related to $KBrO_3$ administration.

We considered the sequence context of G:C > T:A mutations may elicit some specific amino acid changes or nonsense mutations, possibly resulting in more adverse outcomes, particularly when they occur in particular cancer-related genes. According to a human cancer genome study, the ratio of nonsynonymous to synonymous mutations was approximately 1:1 (Hu et al. 2020). However, nonsynonymous mutations were more frequently observed than synonymous mutations in *Mutyh*$^{-/-}$ tumors. Among detected SVNs, 63%, 8.6%, and 28.3% were nonsynonymous, nonsense mutations, and synonymous mutations, respectively. Thus, high-impact mutations for tumor initiation are more likely to be induced by oxidative stress causing defective cell repair for 8-oxoG-mediated mutagenesis. Interestingly, the most frequently observed amino acid change was E > stop, which was often found in *Apc/APC* or *KRAS* in the tumor genome of *Mutyh*$^{-/-}$ mice or MAP (Venesio et al. 2012; Isoda et al. 2014; Viel et al. 2017). Previously, we showed that 87% of tumors derived from $KBrO_3$-treated *Mutyh*$^{-/-}$ mice had nonsense mutations in *Apc* or missense mutations in *Ctnnb1* and that catenin beta 1 (also known as beta-catenin) was accumulated in tumor cell nuclei (Isoda et al. 2014). Herein, three of four tumors had G:C > T:A mutations in specific codons of exon 3 of *Ctnnb1*, which are well-known driver mutations of human colorectal cancer. These mutations change critical amino acids and abrogate GSK3B phosphorylation sites, resulting in constitutively activated growth signaling by altering the Wnt signaling pathway (Krausova and Korinek 2014; Gao et al. 2018).

These observations could explain why MUTYH-defective humans and mice predominantly developed intestinal tumors.

We also showed that chronic exposure to oxidative stress significantly induced intestinal tumors in wild-type mice. When the amount of repair target was exceeded or MUTYH repair ability was inhibited, MF and tumor incidence may increase even in individuals with no *MUTYH* mutations.

In conclusion, we showed that oxidative stress increases the risk of intestinal tumor development by promoting somatic mutation generation via 8-oxoG-mediated mutagenesis, particularly under MUTYH-deficient conditions. However, further studies are needed to investigate how common these observations are in other types of cancer.

Methods

Mice and $KBrO_3$ administration

The *Mutyh* gene knockout mouse line was previously established (Sakamoto et al. 2007) and maintained by backcrossing with C57BL/6Jc, purchased from CLEA Japan. *Mutyh* heterozygous female and male mice were mated to generate congenic *Mutyh*$^{+/+}$, *Mutyh*$^{+/-}$, and *Mutyh*$^{-/-}$ mice for the tumor experiments. The *rpsL* transgenic (Tg) mice (Gondo et al. 1996; Egashira et al. 2002) were used for the somatic mutation assay. *Mutyh*$^{+/+}$/*rpsL*-Tg and *Mutyh*$^{-/-}$/*rpsL*-Tg mice were obtained by mating *Mutyh*$^{+/-}$/*rpsL*-Tg female and male mice. For tumor analysis, mice were fed regular water (reverse osmosis water) or $KBrO_3$-containing water (0.05%, 0.1%, 0.15%, and 0.2%) from 4 wk of age and until 16 wk. For mutation analysis, mice were given regular water for 2 wk after 4 wk $KBrO_3$ administration (Fig. 1A). $KBrO_3$ (Merck) was dissolved in distilled water at appropriate concentrations (g/vol) and stirred for 30 min. Freshly prepared $KBrO_3$ solution in a bottle was set on a cage once a week. All mice were maintained in a specific-pathogen-free facility at controlled temperature and humidity (20°C–26°C, 60%). Animal care and procedures were approved by the institutional animal care and use committee of Kyushu University (approval nos. A22-027, A20-089, A30-147, A28-112). All experiments were performed according to the guidelines for proper conduct of animal experiments of the Science Council of Japan.

Pathological analysis

Pathological samples of full-length small intestinal tissue were prepared using our in-house stretch-and-roll (StR) protocol (for details, see Supplemental Methods). Briefly, the resected small intestine was cleansed to remove contents and then placed in a long plastic tube filled with 10% formalin to straighten it. After 16 h of fixation, the specimen was incised longitudinally, rolled up from one side, and embedded in a paraffin block. These samples were sectioned into 4-µm-thick slices and stained with hematoxylin and eosin (HE). The tumor frequency was evaluated using the flattened specimens fixed in this manner, observed under a stereomicroscope. Tumors with a diameter >1 mm were counted.

Mutation assay by *rpsL*-Tg mice

Tissue specimens resected from *rpsL*-Tg mice were immediately frozen in liquid nitrogen and stored in a −80°C deep freezer until genomic DNA extraction. The *rpsL* mutation assay was performed following methods described previously (Egashira et al. 2002; Isoda et al. 2014), with some modifications (for details, see Supplemental Methods).

WES and detection of somatic mutations

Intestinal tumors and heart tissues isolated from two $KBrO_3$-treated *Mutyh*$^{-/-}$ mice (two tumors and one heart from each mouse) were subjected to WES. Genomic DNA was extracted from the tissue samples using the QIAamp fast DNA tissue kit (Qiagen). The target exon regions (46.9 Mb) were captured using the SureSelectXT mouse all exon kit (Agilent Technologies). Samples were sequenced on the HiSeq 2000 platform (Illumina) with 100-bp paired ends or on the NovaSeq 6000 platform (Illumina) with 150-bp paired ends. Sequenced reads were mapped to the mouse reference genome (UCSC mouse GRCm38/mm10, GRCm39/mm39) using BWA-MEM ver.0.7.17 (Li 2013). After applying base quality score recalibration (Lange et al. 2020), somatic mutations were detected using GATK Mutect2 ver.4.2.0.0 (McKenna et al. 2010) in the tumor-normal mode using the heart as the normal reference. Following FilterMutectCalls, an additional filter (total reads 10 or more for normal and tumor, variant reads three or more for tumor, zero for normal) was applied (Lange et al. 2020). Mutations located within Chr M or in the dbSNP database were excluded. Mutations shared by two or more tumors were also excluded. The called variants, along with their filtering information, are detailed in Supplemental Table S3, and VCF files are in Supplemental Files. The prediction of the genetic effects of called variants, including site information, gene annotation, codon change, and amino acid change, was performed using SnpEff ver.5.1 (Cingolani et al. 2012). The scripts used in the analysis are available in Supplemental Code.

Mutation pattern analysis

The mutation pattern based on 96 trinucleotides type was analyzed using MutationalPatterns ver.3.8.1 (Fleming and Burrows 2023) and Sigprofiler MatirixGenerator ver.1.2 (Islam et al. 2022). The lists of somatic mutations in the human MAP tumor were adapted from Pilati et al. (2017). The list of germline mutations identified from the TOY mice line was adapted from our previous report (Ohno et al. 2014). Mutational signature data (mm10, *Mus musculus*, version 3.3 and v2.0) were downloaded from COSMIC website (https://cancer.sanger.ac.uk/signatures/downloads/). The mutation pattern of tumor WES, human MAP tumor, and *rpsL* assay data were normalized to the mouse genomic trinucleotide frequency using SigsPack ver.12.0 (Schumann et al. 2019).

Statistical analysis

Statistical analysis and data plotting were performed using JMP Pro 15 (SAS Institute) and Microsoft Excel. Mean tumor number, namely, tumor frequency, was calculated as the number of tumors detected in each experimental group divided by the number of mice used. The correlation between tumor frequency or MF and $KBrO_3$ dose was determined using the Spearman's rank correlation test (Supplemental Table S1). Tumor frequency, total MF, and by-type MF in each mouse were used. For tumor prevalence, the ratio of the number of tumor-bearing mice to the total number of mice in each experimental group was used. To test differences in MFs in the control and $KBrO_3$-treated groups in *Mutyh*$^{+/+}$ and *Mutyh*$^{-/-}$ mice, the Steel's test was performed using total MF or by-type MF (Fig. 3A–G).

Data access

All raw and processed sequencing data generated in this study have been submitted to the NCBI BioProject database (https://www.ncbi.nlm.nih.gov/bioproject/) under accession number PRJDB15815.

Competing interest statement

The authors declare no competing interests.

Acknowledgments

This work was partly supported by Grant-in-Aid for Scientific Research (Japan Society for the Promotion of Science) grant numbers JP25241012, JP16H05109, JP20012037, JP26281022, JP22K11733, and JP20H03254. We thank Kosuke Teshima and Yuichiro Hara for their variable advice for sequence data analysis. We thank Kuniko Ishihara for technical support. Computations were partially performed on the National Institute of Genetics supercomputer at the Research Organization of Information and Systems, National Institute of Genetics.

Author contributions: M.O., Yo.N., and T.T. designed the research. Yu.N. provided mice strain information. M.O., N.T., F.S., K.Y., and K.H. performed the experiments and data analyses. M.O. wrote the paper. Y.A. and T.N. provided critical suggestions during manuscript preparation. All authors read and approved the final manuscript.

References

Al-Tassan N, Chmiel NH, Maynard J, Fleming N, Livingston AL, Williams GT, Hodges AK, Davies DR, David SS, Sampson JR, et al. 2002. Inherited variants of MYH associated with somatic G:C→T:A mutations in colorectal tumors. *Nat Genet* **30:** 227–232. doi:10.1038/ng828

Alexandrov LB, Nik-Zainal S, Wedge DC, Campbell PJ, Stratton MR. 2013. Deciphering signatures of mutational processes operative in human cancer. *Cell Rep* **3:** 246–259. doi:10.1016/j.celrep.2012.12.008

Ames BN. 1983. Dietary carcinogens and anticarcinogens. Oxygen radicals and degenerative diseases. *Science* **221:** 1256–1264. doi:10.1126/science.6351251

Aoki Y, Taniguchi Y, Matsumoto M, Matsumoto M, Ohno M, Masumura K, Sasaki S, Tsuzuki T, Yamamoto M, Nohmi T. 2020. Oxidative-stress-driven mutagenesis in the small intestine of the *gpt* δ mouse induced by oral administration of potassium bromate. *Mutat Res Genet Toxicol Environ Mutagen* **850–851:** 503136. doi:10.1016/j.mrgentox.2020.503136

Boiteux S, Coste F, Castaing B. 2017. Repair of 8-oxo-7,8-dihydroguanine in prokaryotic and eukaryotic cells: properties and biological roles of the Fpg and OGG1 DNA *N*-glycosylases. *Free Radic Biol Med* **107:** 179–201. doi:10.1016/j.freeradbiomed.2016.11.042

Cingolani P, Platts A, Wang le L, Coon M, Nguyen T, Wang L, Land SJ, Lu X, Ruden DM. 2012. A program for annotating and predicting the effects of single nucleotide polymorphisms, SnpEff: SNPs in the genome of *Drosophila melanogaster* strain w1118; iso-2; iso-3. *Fly (Austin)* **6:** 80–92. doi:10.4161/fly.19695

Egashira A, Yamauchi K, Yoshiyama K, Kawate H, Katsuki M, Sekiguchi M, Sugimachi K, Maki H, Tsuzuki T. 2002. Mutational specificity of mice defective in the MTH1 and/or the MSH2 genes. *DNA Repair (Amst)* **1:** 881–893. doi:10.1016/S1568-7864(02)00113-1

Evans EJ, Degregori J. 2021. Cells with cancer-associated mutations overtake our tissues as we age. *Aging and Cancer* **2:** 82–97. doi:10.1002/aac2.12037

Fleming AM, Burrows CJ. 2021. Oxidative stress-mediated epigenetic regulation by G-quadruplexes. *NAR Cancer* **3:** zcab038. doi:10.1093/narcan/zcab038

Fleming AM, Burrows CJ. 2023. DNA modifications walk a fine line between epigenetics and mutagenesis. *Nat Rev Mol Cell Biol* **24:** 449–450. doi:10.1038/s41580-023-00590-2

Foster PL, Lee H, Popodi E, Townes JP, Tang H. 2015. Determinants of spontaneous mutation in the bacterium *Escherichia coli* as revealed by whole-genome sequencing. *Proc Natl Acad Sci* **112:** E5990–E5999. doi:10.1073/pnas.1512136112

Gao C, Wang Y, Broaddus R, Sun L, Xue F, Zhang W. 2018. Exon 3 mutations of *CTNNB1* drive tumorigenesis: a review. *Oncotarget* **9:** 5492–5508. doi:10.18632/oncotarget.23695

Gondo Y, Shioyama Y, Nakao K, Katsuki M. 1996. A novel positive detection system of in vivo mutations in *rpsL* (*strA*) transgenic mice. *Mutat Res* **360:** 1–14. doi:10.1016/S0165-1161(96)90231-9

Grasso F, Giacomini E, Sanchez M, Degan P, Gismondi V, Mazzei F, Varesco L, Viel A, Bignami M. 2014. Genetic instability in lymphoblastoid cell lines expressing biallelic and monoallelic variants in the human *MUTYH* gene. *Hum Mol Genet* **23:** 3843–3852. doi:10.1093/hmg/ddu097

Hu Z, Li Z, Ma Z, Curtis C. 2020. Multi-cancer analysis of clonality and the timing of systemic spread in paired primary tumors and metastases. *Nat Genet* **52:** 701–708. doi:10.1038/s41588-020-0628-z

Islam SMA, Diaz-Gay M, Wu Y, Barnes M, Vangara R, Bergstrom EN, He Y, Vella M, Wang J, Teague JW et al. 2022. Uncovering novel mutational signatures by *de novo* extraction with SigProfilerExtractor. *Cell Genom* **2**. doi:10.1016/j.xgen.2022.100179

Isoda T, Nakatsu Y, Yamauchi K, Piao J, Yao T, Honda H, Nakabeppu Y, Tsuzuki T. 2014. Abnormality in Wnt signaling is causatively associated with oxidative stress-induced intestinal tumorigenesis in MUTYH-null mice. *Int J Biol Sci* **10:** 940–947. doi:10.7150/ijbs.9241

Kasai H, Nishimura S. 1984. Hydroxylation of deoxyguanosine at the C-8 position by ascorbic acid and other reducing agents. *Nucleic Acids Res* **12:** 2137–2145. doi:10.1093/nar/12.4.2137

Krausova M, Korinek V. 2014. Wnt signaling in adult intestinal stem cells and cancer. *Cell Signal* **26:** 570–579. doi:10.1016/j.cellsig.2013.11.032

Lange S, Engleitner T, Mueller S, Maresch R, Zwiebel M, González-Silva L, Schneider G, Banerjee R, Yang F, Vassiliou GS, et al. 2020. Analysis pipelines for cancer genome sequencing in mice. *Nat Protoc* **15:** 266–315. doi:10.1038/s41596-019-0234-7

Li H. 2013. Aligning sequence reads, clone sequences and assembly contigs with BWA-MEM. arXiv:1303.3997v2 [q-bio.GN].

Lubbe SJ, Di Bernardo MC, Chandler IP, Houlston RS. 2009. Clinical implications of the colorectal cancer risk associated with *MUTYH* mutation. *J Clin Oncol* **27:** 3975–3980. doi:10.1200/JCO.2008.21.6853

Maynard S, Schurman SH, Harboe C, de Souza-Pinto NC, Bohr VA. 2009. Base excision repair of oxidative DNA damage and association with cancer and aging. *Carcinogenesis* **30:** 2–10. doi:10.1093/carcin/bgn250

McGoldrick JP, Yeh YC, Solomon M, Essigmann JM, Lu AL. 1995. Characterization of a mammalian homolog of the *Escherichia coli* MutY mismatch repair protein. *Mol Cell Biol* **15:** 989–996. doi:10.1128/MCB.15.2.989

McKenna A, Hanna M, Banks E, Sivachenko A, Cibulskis K, Kernytsky A, Garimella K, Altshuler D, Gabriel S, Daly M, et al. 2010. The genome analysis toolkit: a MapReduce framework for analyzing next-generation DNA sequencing data. *Genome Res* **20:** 1297–1303. doi:10.1101/gr.107524.110

Nohmi T. 2018. Thresholds of genotoxic and non-genotoxic carcinogens. *Toxicol Res* **34:** 281–290. doi:10.5487/TR.2018.34.4.281

Ohno M. 2019. Spontaneous de novo germline mutations in humans and mice: rates, spectra, causes and consequences. *Genes Genet Syst* **94:** 13–22. doi:10.1266/ggs.18-00015

Ohno M, Miura T, Furuichi M, Tominaga Y, Tsuchimoto D, Sakumi K, Nakabeppu Y. 2006. A genome-wide distribution of 8-oxoguanine correlates with the preferred regions for recombination and single nucleotide polymorphism in the human genome. *Genome Res* **16:** 567–575. doi:10.1101/gr.4769606

Ohno M, Sakumi K, Fukumura R, Furuichi M, Iwasaki Y, Hokama M, Ikemura T, Tsuzuki T, Gondo Y, Nakabeppu Y. 2014. 8-Oxoguanine causes spontaneous de novo germline mutations in mice. *Sci Rep* **4:** 4689. doi:10.1038/srep04689

Pilati C, Shinde J, Alexandrov LB, Assié G, André T, Helias-Rodzewicz Z, Ducoudray R, Le Corre D, Zucman-Rossi J, Emile JF, et al. 2017. Mutational signature analysis identifies *MUTYH* deficiency in colorectal cancers and adrenocortical carcinomas. *J Pathol* **242:** 10–15. doi:10.1002/path.4880

Poulsen M, Bisgaard M. 2008. MUTYH associated polyposis (MAP). *Curr Genomics* **9:** 420–435. doi:10.2174/138920208785699562

Radicella JP, Dherin C, Desmaze C, Fox MS, Boiteux S. 1997. Cloning and characterization of *hOGG1*, a human homolog of the *OGG1* gene of *Saccharomyces cerevisiae*. *Proc Natl Acad Sci* **94:** 8010–8015. doi:10.1073/pnas.94.15.8010

Rashid M, Fischer A, Wilson CH, Tiffen J, Rust AG, Stevens P, Idziaszczyk S, Maynard J, Williams GT, Mustonen V, et al. 2016. Adenoma development in familial adenomatous polyposis and *MUTYH*-associated polyposis: somatic landscape and driver genes. *J Pathol* **238:** 98–108. doi:10.1002/path.4643

Risques RA, Kennedy SR. 2018. Aging and the rise of somatic cancer-associated mutations in normal tissues. *PLoS Genet* **14:** e1007108. doi:10.1371/journal.pgen.1007108

Robinson PS, Thomas LE, Abascal F, Jung H, Harvey LMR, West HD, Olafsson S, Lee BCH, Coorens THH, Lee-Six H, et al. 2022. Inherited MUTYH mutations cause elevated somatic mutation rates and distinctive mutational signatures in normal human cells. *Nat Commun* **13:** 3949. doi:10.1038/s41467-022-31341-0

Rosenquist TA, Zharkov DO, Grollman AP. 1997. Cloning and characterization of a mammalian 8-oxoguanine DNA glycosylase. *Proc Natl Acad Sci* **94:** 7429–7434. doi:10.1073/pnas.94.14.7429

Ruggieri V, Pin E, Russo MT, Barone F, Degan P, Sanchez M, Quaia M, Minoprio A, Turco E, Mazzei F, et al. 2013. Loss of MUTYH function in human cells leads to accumulation of oxidative damage and genetic instability. *Oncogene* **32:** 4500–4508. doi:10.1038/onc.2012.479

Russo MT, De Luca G, Casorelli I, Degan P, Molatore S, Barone F, Mazzei F, Pannellini T, Musiani P, Bignami M. 2009. Role of MUTYH and MSH2 in the control of oxidative DNA damage, genetic instability, and tumorigenesis. *Cancer Res* **69:** 4372–4379. doi:10.1158/0008-5472.CAN-08-3292

Sakamoto K, Tominaga Y, Yamauchi K, Nakatsu Y, Sakumi K, Yoshiyama K, Egashira A, Kura S, Yao T, Tsuneyoshi M, et al. 2007. MUTYH-null mice are susceptible to spontaneous and oxidative stress–induced intestinal tumorigenesis. *Cancer Res* **67:** 6599–6604. doi:10.1158/0008-5472.CAN-06-4802

Sakumi K, Tominaga Y, Furuichi M, Xu P, Tsuzuki T, Sekiguchi M, Nakabeppu Y. 2003. *Ogg1* knockout-associated lung tumorigenesis and its suppression by *Mth1* gene disruption. *Cancer Res* **63:** 902–905.

Sassa A, Beard WA, Prasad R, Wilson SH. 2012. DNA sequence context effects on the glycosylase activity of human 8-oxoguanine DNA glycosylase. *J Biol Chem* **287:** 36702–36710. doi:10.1074/jbc.M112.397786

Sauer H, Wartenberg M, Hescheler J. 2001. Reactive oxygen species as intracellular messengers during cell growth and differentiation. *Cell Physiol Biochem* **11:** 173–186. doi:10.1159/000047804

Schumann F, Blanc E, Messerschmidt C, Blankenstein T, Busse A, Beule D. 2019. SigsPack, a package for cancer mutational signatures. *BMC Bioinformatics* **20:** 450. doi:10.1186/s12859-019-3043-7

Shibutani S, Takeshita M, Grollman AP. 1991. Insertion of specific bases during DNA synthesis past the oxidation-damaged base 8-oxodG. *Nature* **349:** 431–434. doi:10.1038/349431a0

Sies H. 2015. Oxidative stress: a concept in redox biology and medicine. *Redox Biol* **4:** 180–183. doi:10.1016/j.redox.2015.01.002

Sugiyama H, Saito I. 1996. Theoretical studies of GG-specific photocleavage of DNA via electron transfer: significant lowering of ionization potential and 5′-localization of HOMO of stacked GG bases in B-form DNA. *J Am Chem Soc* **118:** 7063–7068. doi:10.1021/ja9609821

Tajiri T, Maki H, Sekiguchi M. 1995. Functional cooperation of MutT, MutM and MutY proteins in preventing mutations caused by spontaneous oxidation of guanine nucleotide in *Escherichia coli*. *Mutat Res* **336:** 257–267. doi:10.1016/0921-8777(94)00062-B

Tsuzuki T, Nakatsu Y, Nakabeppu Y. 2007. Significance of error-avoiding mechanisms for oxidative DNA damage in carcinogenesis. *Cancer Sci* **98:** 465–470. doi:10.1111/j.1349-7006.2007.00409.x

Venesio T, Balsamo A, D'Agostino VG, Ranzani GN. 2012. MUTYH-associated polyposis (MAP), the syndrome implicating base excision repair in inherited predisposition to colorectal tumors. *Front Oncol* **2:** 83. doi:10.3389/fonc.2012.00083

Viel A, Bruselles A, Meccia E, Fornasarig M, Quaia M, Canzonieri V, Policicchio E, Urso ED, Agostini M, Genuardi M, et al. 2017. A specific mutational signature associated with DNA 8-oxoguanine persistence in MUTYH-defective colorectal cancer. *EBioMedicine* **20:** 39–49. doi:10.1016/j.ebiom.2017.04.022

Waris G, Ahsan H. 2006. Reactive oxygen species: role in the development of cancer and various chronic conditions. *J Carcinog* **5:** 14. doi:10.1186/1477-3163-5-14

Watanabe T, Nunoshiba T, Kawata M, Yamamoto K. 2001. An *in vivo* approach to identifying sequence context of 8-oxoguanine mutagenesis. *Biochem Biophys Res Commun* **284:** 179–184. doi:10.1006/bbrc.2001.4946

Xie Y, Yang H, Cunanan C, Okamoto K, Shibata D, Pan J, Barnes DE, Lindahl T, McIlhatton M, Fishel R, et al. 2004. Deficiencies in mouse *Myh* and *Ogg1* result in tumor predisposition and G to T mutations in codon 12 of the *K-ras* oncogene in lung tumors. *Cancer Res* **64:** 3096–3102. doi:10.1158/0008-5472.CAN-03-3834

Received July 25, 2023; accepted in revised form January 2, 2024.

Oxidative stress accelerates intestinal tumorigenesis by enhancing 8-oxoguanine-mediated mutagenesis in MUTYH-deficient mice

Mizuki Ohno, Noriko Takano, Kyoko Hidaka, et al.

Genome Res. published online January 30, 2024
Access the most recent version at doi:10.1101/gr.278326.123